Supplementary Materials for

Cortical subnetworks encode context of a visual stimulus

Jordan P. Hamm, Yuriy Shymkiv, Shuting Han, Weijian Yang, Rafael Yuste

Correspondence to: rmy5@columbia.edu

This PDF file includes:

Materials and Methods

Animals, Surgery, and Training

All experimental procedures were approved by and carried out in accordance with Columbia University institutional animal care guidelines. Experiments were performed on adult C57BL/6 mice (n=44; Jackson Laboratory, 22-32g) at the age of postnatal day (P) P60-P90. Virus injection, head plate fixation, and skull-thinning/craniotomy were carried out in that order over the course of 4 weeks. For virus injection, mice were anesthetized with isoflurane (initially 3% (partial pressure in air) and reduced to 1-2%). A small window was made through the skull above left V1 (coordinates from lambda: X=-2500, Y=200, Z=-250 μm; n=21), left ACA (from bregma: -300, 600, -900 μm; n=19), or left dLGN (from bregma: -2200, 2300, 2500 μm; n=4 mice) using a dental drill taking care not to pierce the dura mater. A glass capillary pulled to a sharp micropipette was advanced with the stereotaxic instrument, and 75ul solution of 1:1 diluted AAV1-Syn-GCaMP6s (obtained from the University of Pennsylvania Vector Core; n=20) or AAV1-CAG-ArchT-tdTomato (UNC GTC vector core; n=7 mice) was injected into putative layer 2/3 over a 5 min period at a depth of 200-300 μm from the pial surface using a UMP3 microsyringe pump (World Precision Instruments). Additionally, for the volumetric imaging experiments, in 4 mice AAV1-Syn-jRGECO1b was injected at 500 μm deep in V1, together with AAV9-Syn-GCaMP6s at 250 μm. Immediately after this procedure, a titanium head plate was attached to the skull centered on V1 using dental cement. Mice were allowed to recover for at least 5 days in their home cage. Mice were given analgesics (5mg/kg carprofen I.P.). Approximately 2-3 weeks after virus injection, mice were accustomed to experimenter handling, including brief head-restraint periods, until mice showed non-stressed behavior, which usually began on the second day. Mice were accustomed to head fixation as previously described (*1*, *9*). During training sessions and prior to the first imaging session, mice viewed moving square-wave gratings (see below) for stimulus habituation.

Visual Stimulation

Visual stimuli were generated using the MATLAB (MathWorks) Psychophysics Toolbox and displayed on a liquid crystal display monitor (19-inch diameter, 60-Hz refresh rate) positioned 15 cm from the right eye, roughly at 45° to the long axis of the animal (Fig. 1A). Stimuli were static full-field square-wave gratings (100% contrast, 0.04 cycles per degree) oriented in one of 2 separate orientations for the oddball paradigm (45deg and 135deg; 0 deg and 90 deg; counterbalanced across mice) or in 8 orientations for the many-standards control (30, 45, 60, 90, 120, 135, 150, 180 deg). Stimuli were presented for 500 ms followed by an interstimulus interval of 1000-1500 ms of mean luminescence gray screen. In the oddball sessions, the "standard" stimulus was presented at a minimum of 3 sequential trials, followed by a linearly increasing probability of the "target" stimulus on each successive trial to yield an overall 12.5% probability of targets. These sessions lasted 10 minutes, and were repeated with the "standard" and "target" stimuli reversed. In the many-standards sessions, stimuli of 8 separate orientations each occurred at random with a 12.5% probability in a session of 10 minutes. The timing and identity of gratings played in MATLAB were synchronized with image acquisition by outputting an analogue voltage trigger synchronized with stimulus onset and offset and recorded with the imaging computer using Prairie View 5.3. The timing between actual stimulus onset and recorded voltage traces in Prairie View or Plexon software was confirmed beforehand using a photodiode sensor with a reverse biased voltage output recorded by the software in tandem with the MATLAB output triggers.

Two-Photon Calcium Imaging: single plane (n=26 mice).

The activity of cortical neurons was recorded by imaging fluorescence changes under a two-photon microscope (Bruker Ultima In Vivo; Billerica, MA) excited with a Ti:Sapphire laser (Chameleon Ultra II; Coherent) tuned to 940 nm. The laser beam was intensity modulated with a Pockels cell (Conoptics 350-160BK, with 302 RM driver) and scanned with galvometers through a 20× 0.9 N.A.; (Olympus) water immersion objective (Figure 2A-B). To ensure stability of the imaging meniscus for long duration imaging sessions,- a small volume (approx. 1ml) of Aquasonic ultrasound gel (Parker Laboratories Inc.) was centrifuged and dolloped onto a moistened, thinned skull. Scanning and image acquisition were controlled by Prairie View software (3.395 frames per second for 256 × 256 pixels, 1.6 microsecond dwell time per pixel, 200-225 um beneath the pial surface). The Pockels cell blanked the laser outside the imaging field to minimize laser exposure. On both imaging days (before and after treatment) mice were allowed 1 hour on the wheel before imaging began. Sessions started at the same time of day for both sessions within a mouse (starting between 11am and 4pm). Mice and recordings were visually monitored by the experimenter to ensure they were awake during data collection. Locomotion was recorded with an infared LED/photodarlington pair (Honeywell S&C HOA1877-003), which consists of a small c-shaped device positioned at the edge of the rotating wheel (striped with black tape) connected to the imaging computer as an analogue input. Locomotion was detected as voltage detections in the photodarlington readout. While previous work has suggested that locomotion enhances visual processing in V1 in mice(*30*), most of our mice did not exhibit enough locomotion to enable thorough examination of this effect in our chronic models (< 10% of frames). Therefore, when detected, frames or trials during locomotion periods were excluded along with the previous and subsequent 12 frames; this did not change the pattern of effects (*14*).

Two-Photon Calcium Imaging: multiplane/volumetric (n=4 mice).

Two-photon volumetric calcium imaging experiments were carried out with a customized microscope with two excitation lasers: a Ti:Sapphire laser (Chameleon Ultra II, Coherent) at 920 nm, and an amplified fiber laser laser (Fianium) at 1064 nm. The laser power is controlled with two Pockels cells (Conoptics; EO350-160-BK with a 275 driver for 920 nm laser, EO350-105-BK with a 302 RM driver for 1064 nm laser). A 4f system with an offset lens at its intermediate plane was inserted in the 1064 nm laser beam path to provide a ~ 150 μm focus offset from the nominal focus of the objective lens (Olympus XLPlan N, 1.05 NA). In addition, an electrical tunable lens (EL-10-30-C-NIR-LD-MV, Optotune) was inserted in the 920 nm laser beam path, and a spatial light modulator (SLM, HSP512, Meadowlark Optics) in the 1064 nm laser beam path, so that the focal plane of both lasers could be dynamically adjusted. The two laser beams were combined through a dichroic mirror, scanned by resonant galvanometric scanning mirrors (CRS 8K resonant scanning system, 6215H galvanometric mirror, Cambridge Technology), and delivered to two different focal planes. The two focal planes from the two lasers were imaged simultaneously, and volumetric imaging was implemented through a fast-sequential axial switch of the dual plane imaging. The frame rate is 60 frames per second (256x256 pixel imaging). Emission fluorescence was collected through two separate PMTs, with a collection filter of 510 ± 40 nm for the green path, and a 630 ± 75 nm for the red path. ScanImage 2016 (*31*) was used to control the Pockels cells, the focus of the electrically tunable lens and spatial light modulator, the scanning mirrors and the digitizer for data storage. Locomotion of the animals were recorded using a similar approach detailed in the single plane two-photon calcium imaging section.

Image Analysis

Imaging datasets were scored similarly to previous reports (*1*, *14*, *32*, *33*). The raw images were processed to correct translational brain motion artifacts using an in house plugin named "Moco" for ImageJ (*34*, *35*). Then, cell regions of interest (ROIs) were detected semi-automatically for each imaging session and individually confirmed as follows. Mean, standard deviation, and std×skewness projections (pixel-wise) were calculated across all imaging frames (roughly 14000-25000) and plotted for reference. Then, rectangular sections were selected around the apparent cell bodies using a GUI created in MATLAB. A principal components analysis (PCA) was computed on the pixels contained within the sections, and the pixels with weights at least 80% of the maximum of the first PCA component were defined as the ROI and spatially plotted along with the florescence trace averaged across these pixels. Florescence of active cells was then calculated as the average across all pixels within this ROI minus the average of the pixels just outside the selected rectangle, termed the "halo", which excluded pixels from nearby cell bodies. This subtraction removed background contamination from neuropil and nearby cells. Completing this step ensures maximal correspondence between florescence and actual cell spiking (*33*). For a subset of the data (the images acquired with the volumetric multiplane approach, n=4 mice, 8 experiments), a slightly different approach was employed to identify the cell body regions of interest given the vast numbers of cells present. Cell centroids were manually initialized, then cell body masks, fluorescence "signals", and background were automatically modeled using the constrained nonnegative matrix factorization (CNMF) algorithm (*36*), automated for matlab with scripts written in house.

After these steps, each cell outline and trace was manually inspected, and cells with no apparent calcium transients were excluded from further analysis. For the axon imaging experiments, correlations of all remaining traces were computed, and ROI-pairs with correlations above r=.5 were visually inspected in order to rule out multiple ROIs being included in the analysis from the same cell. That is, because multiple boutons or axon segments from the same dLGN or ACA neuron could appear in the same field of view, our goal was to include only one trace from each cell. Traces of ROIs determined to be from the same cell were averaged. This led to the elimination of only about 5% of ROIs. The remaining traces were then filtered with a 1-second lowess envelope (*37*), a regression based smoothing approach which is tolerant of sharply changing baseline values. Finally, the discrete first derivative was scored as delta-f (within cell/single cell comparisons). After averaging over trials, the 250ms prestimulus average for all three stimulus types (control, redundant, deviant) were combined, and the mean and standard deviation was calculated on the delta-f values in this 750ms window for each cell. These values were used to compute a z-scored delta-f for visualizing and combining activity across cells (*1*).

Multielectrode recordings

Extracellular electrophysiological data are reported on 14 mice (8 female, 22-28g) undergoing the virus injection protocol described above. Sixteen-channel linear silicon probes (spaced at 50 Um intervals; model a1x16-3mm50-177, Neuronexus Technologies, Ann Arbor MI) were inserted perpendicular to and with the top electrode aligned just at the pial surface (visually confirmed with an adjustable miniature digital microscope (adafruit)). Recordings were referenced to the headplate, which made contact with the skull and saline meniscus, and were grounded to the stage. Continuous data were acquired with a Plexon MiniDigi amplifier and software (Plexon Inc, Dallas, TX). Local field potential (LFP) signals were filtered from 0.1 to 300Hz, sampled at 1kHz, and analysed as LFP and current source density (see below). Multiunit activity (MUA) was sampled at 40kHz, digitally filtered (300–5000 Hz; bandpass least squares FIR), rectified, and then downsampled to 1 kHz. The result was low-pass filtered at 100Hz (least

squares FIR) to estimate the local population spiking envelope. Locomotion was recorded as described above.

LFP and current source density (CSD) processing and analysis

LFP data were manually prescreened for excessive artifact (e.g. signal greater than 8 standard deviations). Aberrant trials were removed and noisy channels were interpolated if present (never more than 2, and never 2 adjacent channels). Data were then digitally filtered from 0.1 to 300Hz (bandpass least squares FIR) and with a 60Hz notch filter. For analysis of the LFP response, the channel of maximal negative deflection in the first 150 ms post stimulus (typically channel 12-16, or layer 4-5) was selected. Initial demonstration of SSA and deviance detection were established via a "planned comparisons" approach with paired t-tests (one-tailed) on mouse-wise averages. For SSA we compared responses between redundant (using the 4th redundant in order to normalize for trial counts and for relative time during the run) and control stimuli in the early time-range (40-110 ms) most likely to capture SSA (*2*). For deviance processing, we compared responses between deviant and control stimuli in the late time-range (140-300 ms) (*1*). Trial numbers were equated between stimulus conditions. All standard error bars in all figures reflect within-subjects/within-cells standard error (*38*).

For descriptive purposes, average current source density (CSD) was computed from either the average LFP (Fig. S1A) by taking the discrete second derivative across the electrode sites and interpolated to produce a smooth CSD map (*39–41*). Putative laminar subregions (3 channels) were defined based on CSD demarcations previously published and histologically verified in mouse V1(*40*) for each mouse separately based on average CSD plots. The laminar subdivisions served only descriptive purposes in this paper. Average CSD waveforms were averaged over stimulus orientations (Fig S1E) since waveforms did not show robust differences, an expected effect given i) the lack of orientation columns in mouse V1 (*41*) and ii) previous LFP recordings in mouse V1 (*42*). In general, grating evoked averages suggested a laminar distribution of activation in response to grating stimuli, with a current sink beginning in layer 4 with corresponding, sustained sources in layer 2/3 and 5. The LED induced retinal artifact observed in optogenetic experiments (Fig S4B) had a similar distribution, albeit a more focal sink source pattern.

Calcium imaging analysis: single cell effects

Condition averages of normalized delta-f values for redundant (4th in sequence), deviant, and control stimuli were calculated separately for each stimulus type for each neuron. All analyses focused on the first 10-trials to equate across conditions, cells, and mice with varying numbers of available trials. Initial analyses focused on neurons showing, during control or deviant conditions, an average post-stimulus (0-1second) response of 3.1 stdevs above prestimulus baseline (equating to a 1-tailed p-value of .001). Only responses to one stimulus orientation were considered for each cell (i.e. the orientation with greater magnitude). Initial demonstration of SSA and deviance detection were established via a "planned comparisons" approach with paired t-tests (two-tailed) on cell-wise averages of post stimulus activity (0-0.5 sec). For SSA we compared responses between redundant and control stimuli; for deviance processing, we compared responses between deviant and control stimuli.

Calcium imaging analysis: cluster analyses

Average responses to control, redundant, and deviant stimuli averaged over trials and the stimulation period (0-500ms post stimulus) were subjected a series of k-means clustering analyses to determine the number and nature of nascent subgroups with shared context modulated responses. We employed a method previously demonstrated (*14*, *43*) utilizing a

comparison of how much inter-observation (i.e. inter-cell) average response distances are decreased with each added cluster to the solution (from number of clusters k=2 to 8), and a comparison of this curve to a family of 1000 surrogate curves derived from a shuffling procedure (shuffling within cells, across contexts). At each added cluster, we computed the within-cluster between cell distances (i.e. Euclidean distances) in average response space (i.e. control, redundant, deviant), dividing by their decrease from the k-1 solution by the overall within cell distances (k=1; or no clusters), generating a curve for the observed (black line in Fig. 1G) and shuffled solution set (gray line in Fig. 1G). Error bars indicate 3.10 standard deviations from the mean. We identified the highest number of clusters which exceeded 3.10 standard deviations from the mean ($p<.001$) and carried out that analysis as the main solution. When comparing distributions of cluster proportions, a 2Xn chi-squared analysis was carried out on proportion values where n is equal to the number of clusters.

Optogenetic suppression of PFC axons.

A 617-nm High-Power LED coupled to the Ø400 um Core Patch Cable (Thorlabs) was positioned around the cranial window as described previously(*29*). Light intensity at the tip was approximately 4 mW. The tip was coupled to the fiber optic cannula (Thorlabs), and positioned under a 20×water immersion objective (0.95 N.A.; Olympus), to indicate the center of the imaging window. The distance between the cranial window and the tip was adjusted so that the radius of the illumination field was approximately 1mm. The imaging setup, and the space between cranial window and the objective were completely enclosed with blackout fabric (Thorlabs). First, baseline runs (many standards control, oddball, oddball flipped) for each experiment was completed without LED illumination. Then, after 30 minutes, these runs were repeated with the same visual stimuli along with LED illumination occurring every other trial, starting 500ms pre-to 500ms post-visual stimulus onset.

Activity of visual cortical neurons were imaged and processed as described above. Mice with PFC ArchT injections were compared to mice receiving only PFC GCaMP6S injections. Cell-level effects on SSA and deviance detection were analyzed for PFC suppression mice with a 2-by-2 ANOVA on individual cells with STIMTYPE (CONTROL; REDUNDANT [for SSA]) or (CONTROL; DEVIANT [for deviance detection]) and TREATMENT (without LED; with LED) as between subject variables (all cells pre and post included). One-way repeated measures ANOVAs within TREATMENT conditions were used to describe interaction effects (i.e. the presense of SSA and deviance detection before and during stimulation) and, further, two-tailed two sample t-tests were used to determine whether responses to specific stimuli (control, deviant, redundant) were changed by the LED. The same statistical model was used for the control condition to rule out effects of LED illumination on its own.

Histology and imaging

Mice were transcardially perfused with cold PBS and 4% PFA, brains were extracted and incubated in PFA overnight. Next day, brains were washed in PBS for 30 min and cut into 75um free-floating coronal sections (Leica VT1000S). Slices were washed for 10 min in PBS, counterstained with DAPI (1ug/ml), washed in two more times and mounted with Fluoromount-G (ThermoFisher). Brain sections were photographed with Leica M165FC dissection microscope and Hamamatsu ORCA-Flash4.0 camera, or Zeiss LSM 800 confocal microscope. Images were analyzed in ImageJ.

Supplementary Text

Validation of cluster membership

We trained the "clusters" on the odd trials (5 total), and tested their preferences on the even trials (5 total; Figure S2D). Ensemble response averages retained their character and statistical significance (dev-detect cluster: $t(101)=4.5$, $p<.001$ (deviant vs [control+redundant]); gen-adapt cluster: $t(113)=4.17$, $p<.001$ (control vs [deviant+redundant]; no-mod cluster: $t(78)<1.5$, $p>.05$ for both combinations). Second, we recorded the same cells in a separate run 30 minutes later (Figure S2E). Again, ensemble response averages retained their character and statistical significance (dev-detect cluster: $t(92)=2.65$, $p<.01$ (dev vs [cntrl+red]); gen-adapt cluster: $t(59)=2.32$, $p<.05$ (cntrl vs [dev+red]; no-mod cluster: $t(34)<1.5$, $p>.05$ for both combinations). Finally, we sought to determine whether cells within the same clusters showed stronger correlations across the imaging session than cells in separate clusters. Correlation coefficients were calculated for all cell pairs (using all recorded timepoints), compared to a time-shuffled surrogate dataset for each cell pair to derive a Z-score, and then a "within" and a "between" cluster estimate was calculated for each experiment. Indeed, cells within the same cluster showed stronger correlations than cells in different clusters ($t(21)=3.08$, $p<.01$; Fig. S2F; all 23 experiments included from each cluster except 1).

.

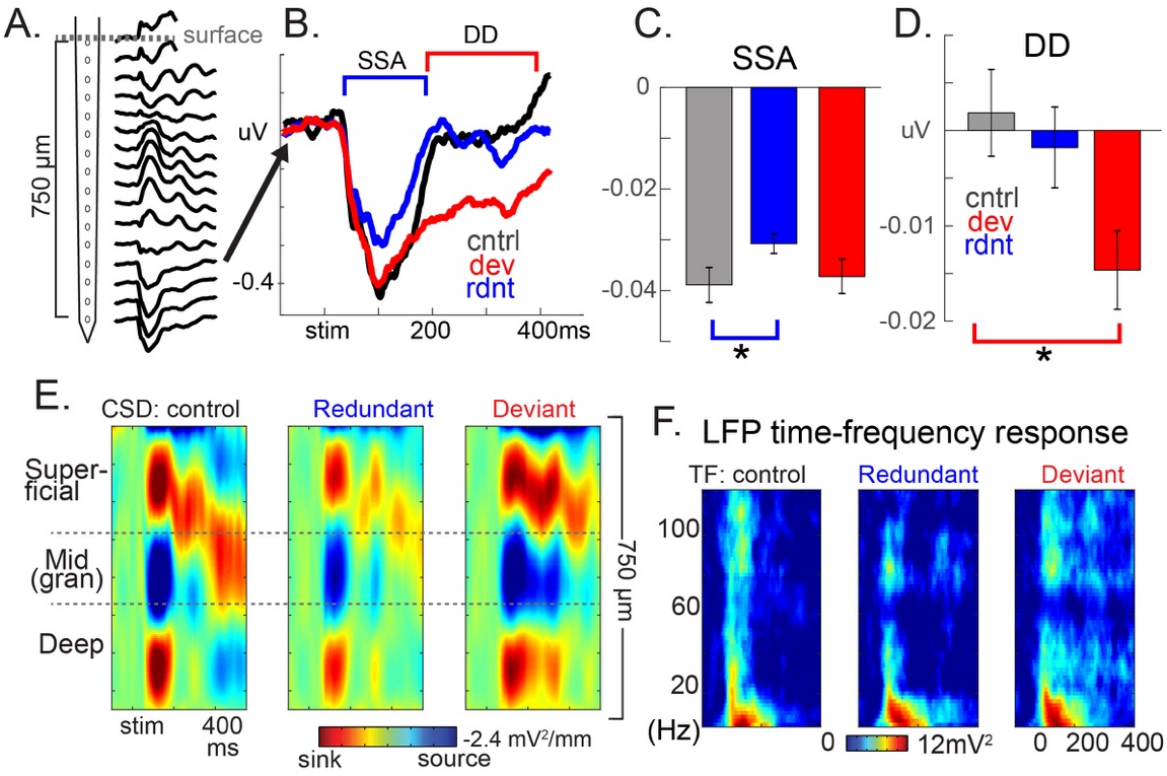

Fig. S1. (A) Local field potential (LFP) recordings across the depth of visual cortex (n=14 mice). (B) Average LFP trace from contact with largest negative deflection for each mouse,

averaged across mice show (C) stimulus specific adaptation (SSA) occurring between 75 and 125ms post stimulus onset (averaged voltage within interval for each mouse; $t(13)^{\text{one-tailed}}$=-1.87, p<.05; rdnt vs cntrl), while (D) deviance detection occurs after 175ms post-stimulus onset($t(13)^{\text{one-tailed}}$=2.18, p<.05; dev vs cntrl). (E) Current source density projection and (F) time frequency decomposition of the same data depict the same pattern of results (*p<.05).

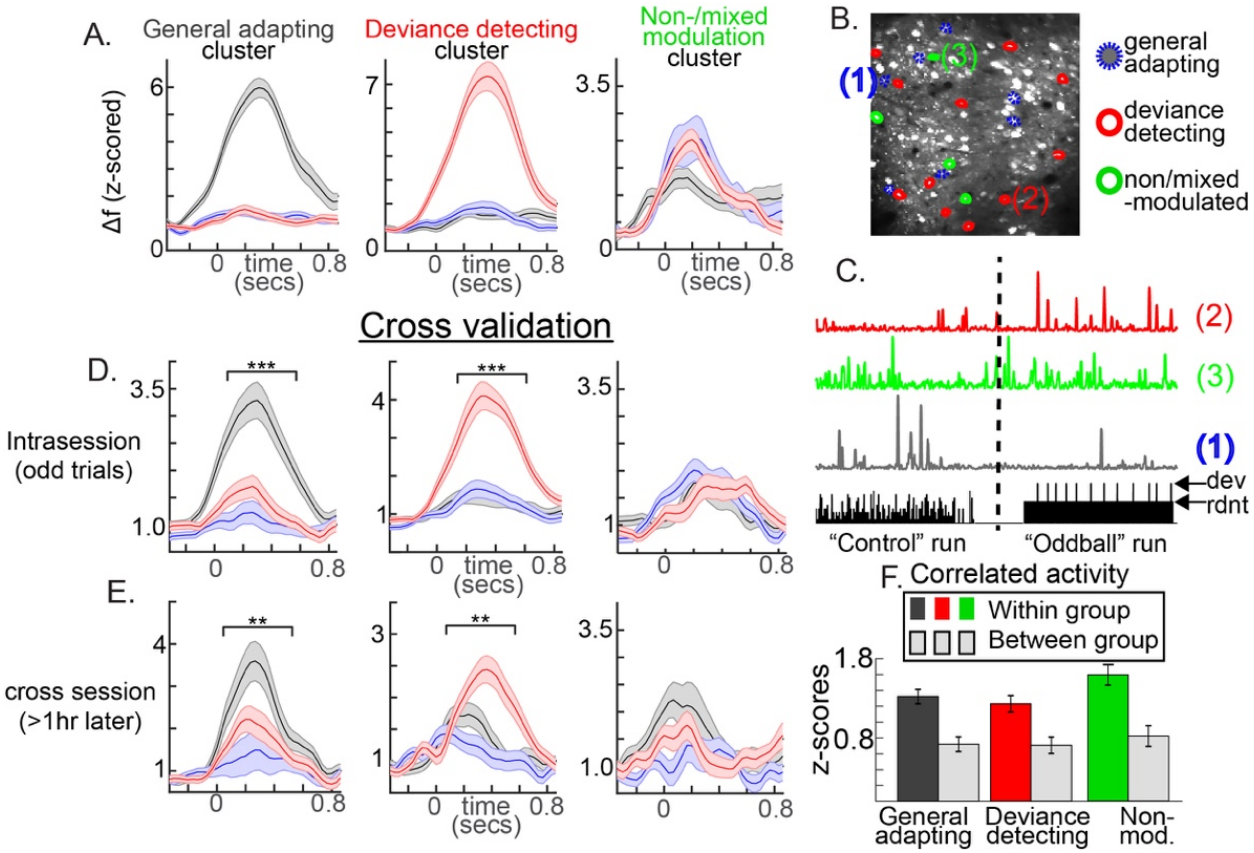

Fig. S2. (A) Averages from the first 5 "even" trials for the three clusters. (B) Average projection from one example mouse show that the somas from the three clusters are spatially intermixed. (C) Delta-f calcium traces from one of each of the above cell types, scaled by their max delta-f, show that activity and signal was stable across both "runs", yet cells simply showed more activity to their preferred context. (D) intrasession cross-validation: average responses from the "odd trials" from the same cells clustered on the "even trials" show the same pattern of activity across contexts. (E) cross session cross-validation: average responses from a subsequent set of runs 30 minutes after completion of the previous oddball run show that clusters are stable for cells which show signal in both sessions. (F) correlated activity across the entire imaging session was stronger within vs between clusters. (***p<.001; **p<.05).

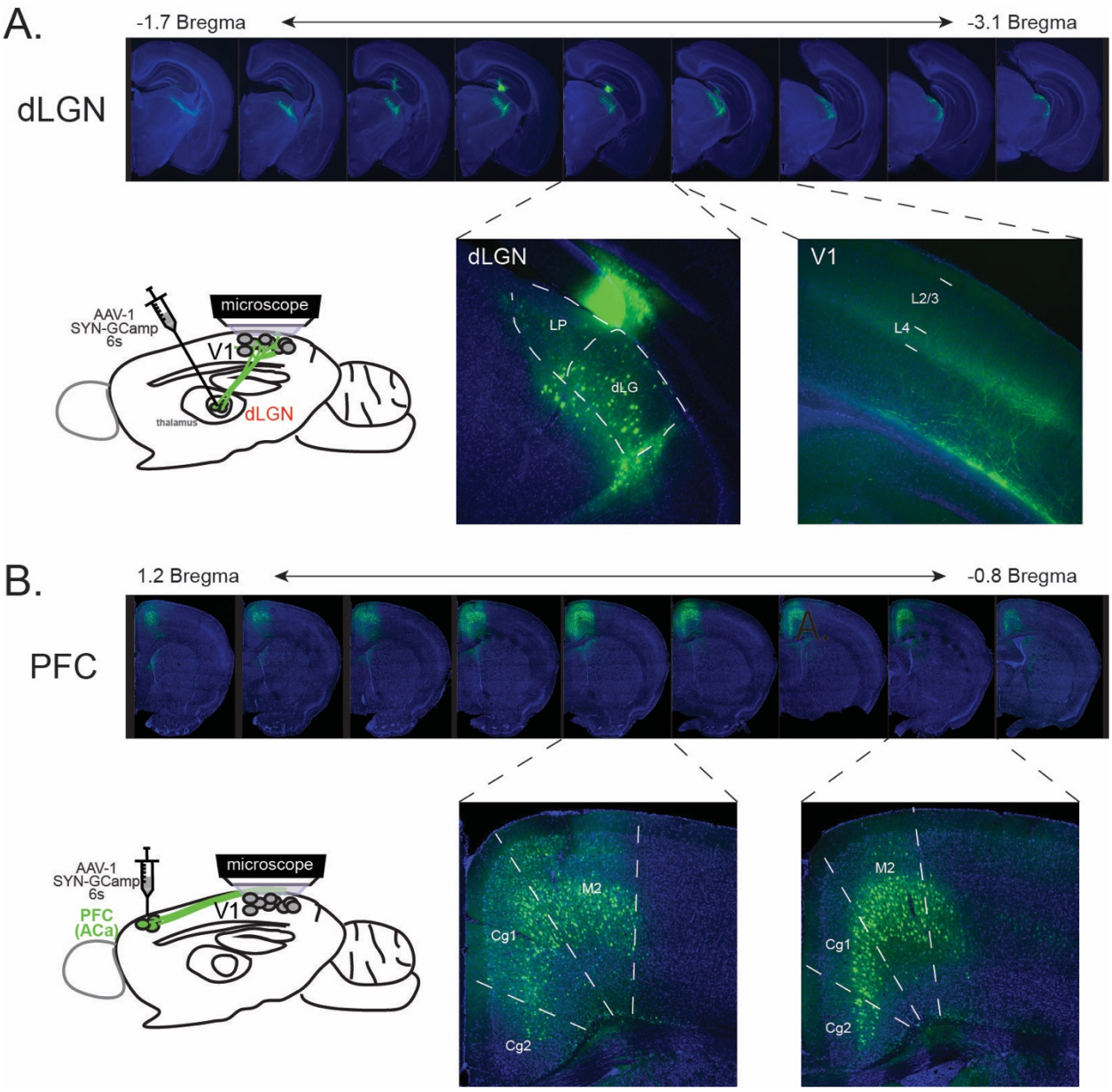

Fig. S3. Histological confirmation of viral injections (A) Top, series of coronal sections describing the expression of calcium indicator after injections targeting dLGN. Bottom, schematic of viral injection to dLGN (left), magnified image of dLGN (center), and axonal inputs to V1 (right). (B) Top, coronal sections of PFC describing the expression of calcium indicator following injections to Cg1. Bottom, schematic of viral injection to Cg1 (left), magnified images of Cg1 (center and right). Although soma from multiple PFC areas expressed GCaMP6s, only neurons from Cg1 are known to project to V1, and so our interpretations focus on this area. Abbreviations: dLGN, dorsal lateral geniculate nucleus; V1, primary visual cortex; LP lateral posterior thalamic nucleus; Cg1, cingulate cortex 1; Cg2, cingulate cortex 2; M2, secondary motor cortex.

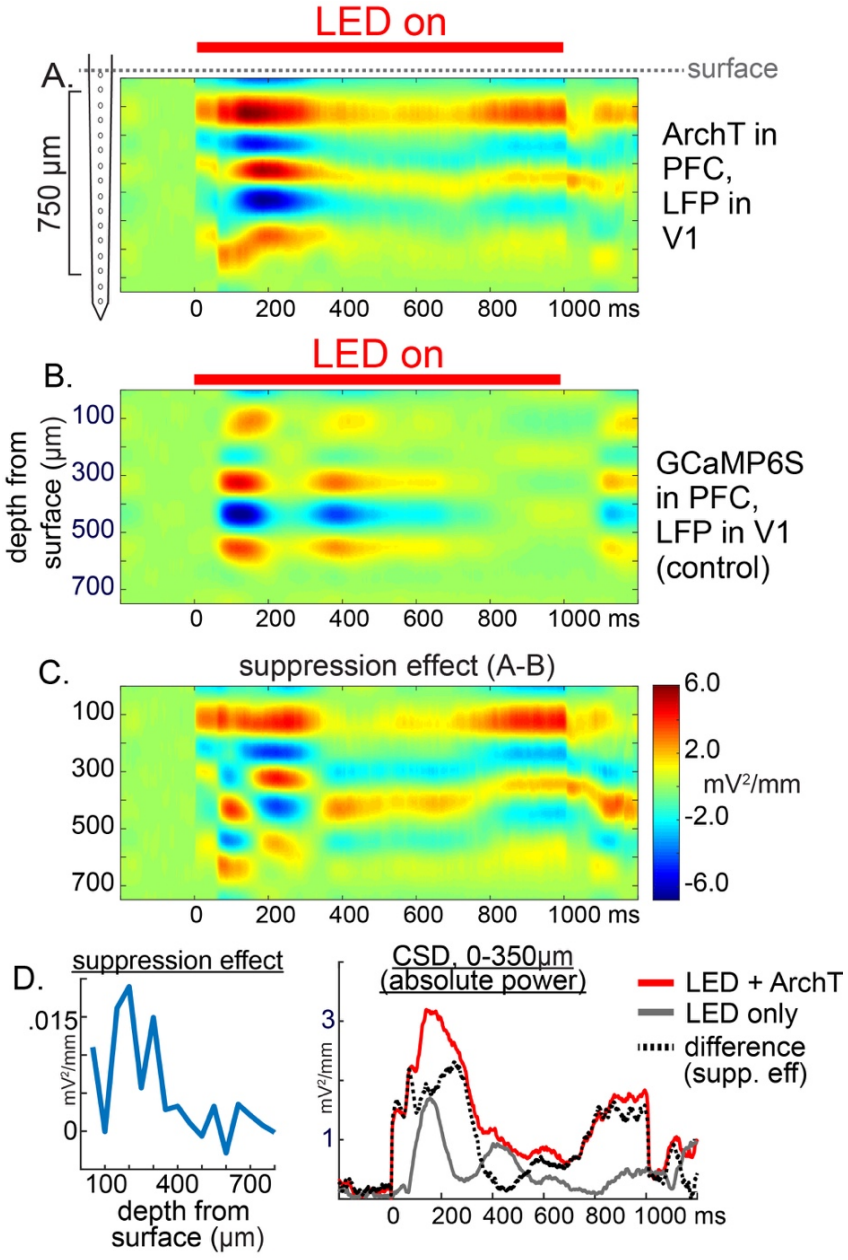

Fig. S4. Multielectrode demonstration of ArchT activation. A) Current source density (CSD) plot averaged over 7 mice, 20 trials each, in the presence of ArchT and (B) absence (5 mice). (C) Subtracting B from A yields the difference CSD plot. (D) Averaging over the 1000ms time period of illumination from the plot in C shows that the effect was mainly superficial, while (right) taking an absolute value of the plot in C from the top 300um shows the fast timecourse of the ArchT effect relative to the simple visually evoked response.

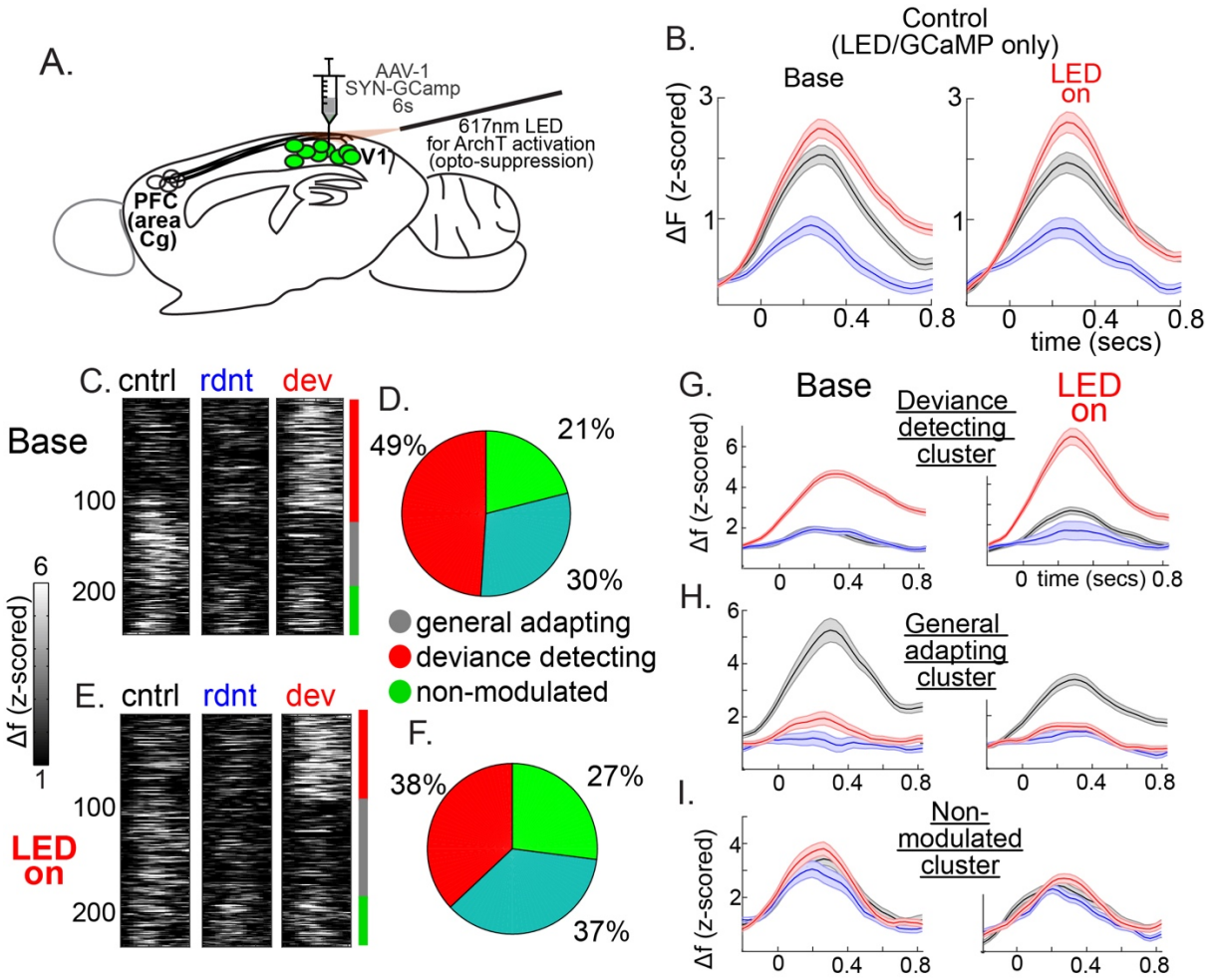

Fig. S5. Optogenetic control experiments show no effect of LED (A) Schematic of viral injections to V1, and (B) Average responses across 239 V1 neurons before (left) and during LED stimulation. (C) pre-LED baseline k-means sorted neuron average responses to stimulus types, and (D) relative proportion of each subcluster. (E,F) same as (C) and (D) but during control LED illumination. (G,H,I) averages across all neurons in each cluster before (left) and during control LED illumination.

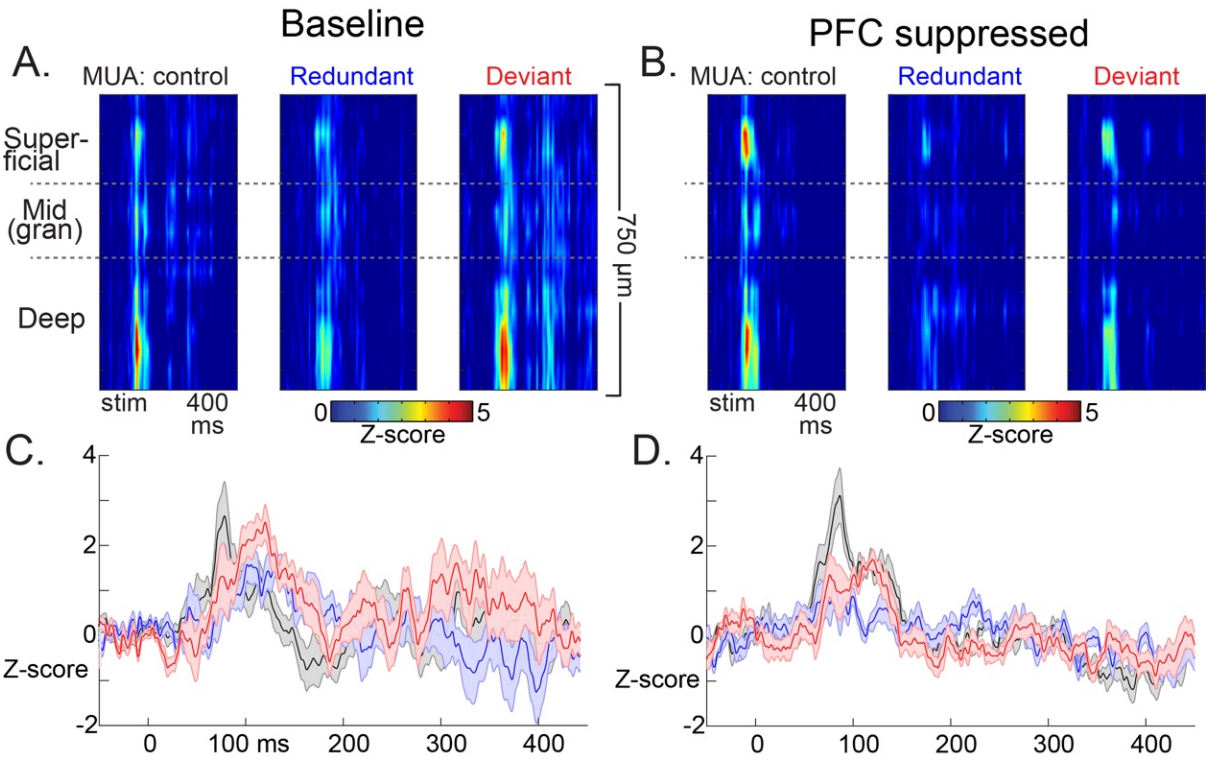

Fig. S6. Electrophysiological confirmation of 2P-Ca++ effects. (A) Trial-averaged multiunit activity (MUA) to stimuli in each context demonstrates enhanced responses to deviant stimuli and decreased responses to redundant stimuli across all depths. (B) PFC suppression eliminates deviance detection by enhancing response in control/neutral context, and decreasing responses in oddball contexts (redundant and deviant). (C,D) activity from (A) and (B) averaged over all electrode contacts. N=6 mice.